Colloids and Surfaces A: Physicochemical and Engineering Aspects 642 (2022) 128653

Contents lists available at ScienceDirect

Colloids and Surfaces A: Physicochemical and Engineering Aspects

journal homepage: www.elsevier.com/locate/colsurfa

Novel strategy of highly efficient solar-driven water evaporation using MWCNTs-ZrO_2-Ni@CQDs composites as photothermal materials

Riski Titian Ginting [a,*], Hairus Abdullah [b], Erman Taer [c], Oktovin Purba [d], Despaleri Perangin-angin [a]

[a] Department of Electrical Engineering, Universitas Prima Indonesia, Medan, Indonesia
[b] Department of Industrial Engineering, Universitas Prima Indonesia, Medan, Indonesia
[c] Department of Physics, Faculty of Mathematic and Natural Sciences, University of Riau, Simpang Baru, Riau 28293, Indonesia
[d] Nanomaterials for Renewable Energy Laboratory, CV. Inovasi Teknologi Nano, Medan, Indonesia

GRAPHICAL ABSTRACT

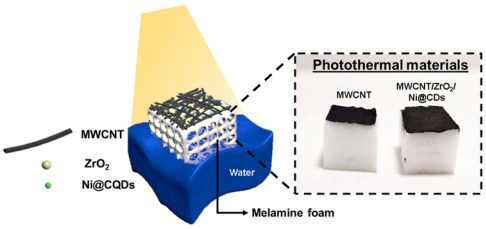

ARTICLE INFO

Keywords:
Carbon nanotube
ZrO_2
Nickel doped carbon dot
Solar driven water evaporation

ABSTRACT

Solar-driven water evaporation is a promising technology for high efficiency water purification by absorbing solar energy and converted into localized heat. Herein, we report a low-cost approach for developing a novel photothermal materials based on combination of ZrO_2 nanoparticles (NPs) with Ni doped carbon quantum dots (Ni@CQDs) and multi-walled carbon nanotube (MWCNT) coated on melamine foam (MF) surface. The formation of Ni@CQDs was confirmed by red-shift absorbance and fluorescence. Moreover, the shift in XRD diffraction angle indicated the Ni@CQDs incorporated into the ZrO_2 and carbon framework of MWCNT. The composite absorber demonstrates excellent solar-water evaporation rate of 1.95 kg m^{-2} h^{-1} and high evaporation efficiency of 89.5%, which is ten-fold improvement as compared to pure water (0.19 kg m^{-2} h^{-1}) under 1-Sun irradiation. The enhancement in evaporation rate is mainly attributed to the strong light absorption of 94% and extremely low thermal conductivity of MWCNT/ZrO_2/Ni@CQDs (0.038 W m^{-1} K^{-1}). The composite absorber capable of continuous operation of 6 cycles under 1-Sun irradiation, indicates high durability and completely reduced organic dyes (99.8%). Accordingly, the novel design of MWCNT/ZrO_2/Ni@CQDs as composite absorber as high performance solar-driven water evaporation and wastewater purification.

* Corresponding author.
E-mail address: titiangt@unprimdn.ac.id (R.T. Ginting).

https://doi.org/10.1016/j.colsurfa.2022.128653
Received 24 November 2021; Received in revised form 24 January 2022; Accepted 21 February 2022
Available online 24 February 2022

1. Introduction

In the past decades, increasing water pollution and the lack of water for agricultural and economic growth, the clean water scarcity has become an urgent worldwide issue [1]. Solar energy was known as renewable and abundant energy resource, where tremendous effort have been devoted for highly efficient photothermal research with the goal of addressing serious water shortage, solar–thermal conversion with solar-irradiation driven water evaporation is required [2]. The concept of localized interfacial heating has been presented to improve the efficiency of water evaporation system with photothermal materials properties of, and highly efficient photothermal conversion, broad solar absorption, low thermal conductivity, heat management to minimize heat loss, thermal/chemical/photostability for practical applications and efficient water transport to c confirm continuous water vaporization based on porous structure [3]. Recently, several photothermal materials have been developed so far for conversion of solar energy to heat mainly focused on conjugated polymers [4], plasmonic [5], biomass [6], carbon-based [7] and semiconductor materials [8]. Among other materials, carbon nanotubes (CNT) is the most commonly used as photothermal materials due to broadband solar harvesting, low specific heat and stable physicochemical properties [9], however have high thermal conductivity that lead to unnecessary heat dissipation [10]. Therefore, it is essential to obtain CNT with high photothermal conversion capability, while simultaneously low thermal conductivity.

Carbon quantum dots (CQDs) mainly absorb a wide range of solar spectrum, large surface area-to-volume ratio, efficient heat generation and low thermal conductivity, which is beneficial for heat localization for solar water evaporation [11,12]. Previously, CQDs incorporated into wood matrix [12] and polypyrrole/CQDs modified MnO_2 nanowires [13] were reported and demonstrate a significant enhancement in evaporation rate and efficiency. Zirconia oxide nanoparticles (ZrO_2 NPs) show surface hydrophilicity [14], strong and broad visible-light absorption [15], low thermal conductivity [16] and good chemical stability [17]. Accordingly, the combination of CQDs and ZrO_2 NPs for the application of solar driven water generation is worthy to be investigated, since ZrO_2 could act as electron acceptor from CQDs during light illumination process and provides more heat energy into the evaporation system, meanwhile CNT improved the diffused reflection of light.

Herein, a novel combination of multi-walled CNT(MWCNT) with ZrO_2 NPs and Ni doped CQDs (Ni@CQDs) via low-cost hydrothermal method were presented a strategy for improving light absorption and lower thermal conductivity by developing. The composite absorber was brush coated onto melamine foam (MF) surface as light-absorbing layer, where MF substrate guarantee fast water transportation. The composite absorber revealed the MWCNT/ZrO_2/Ni@CQDs highly promising for high water evaporation rate and stable solar-driven water evaporator.

2. Experimental

2.1. Chemicals

Graphitized MWNTs (diameter 8–15 nm) and ZrO_2 NPs (particle size 10–15 nm) were purchased from XFNANO and used without further purification. Glacial acetic acid and nickel chloride hexahydrate was procured from SmartLab, Indonesia. Poly(vinyl) alcohol (PVA) Mw 89,000–98,000 was acquired from Sigma Aldrich, Singapore.

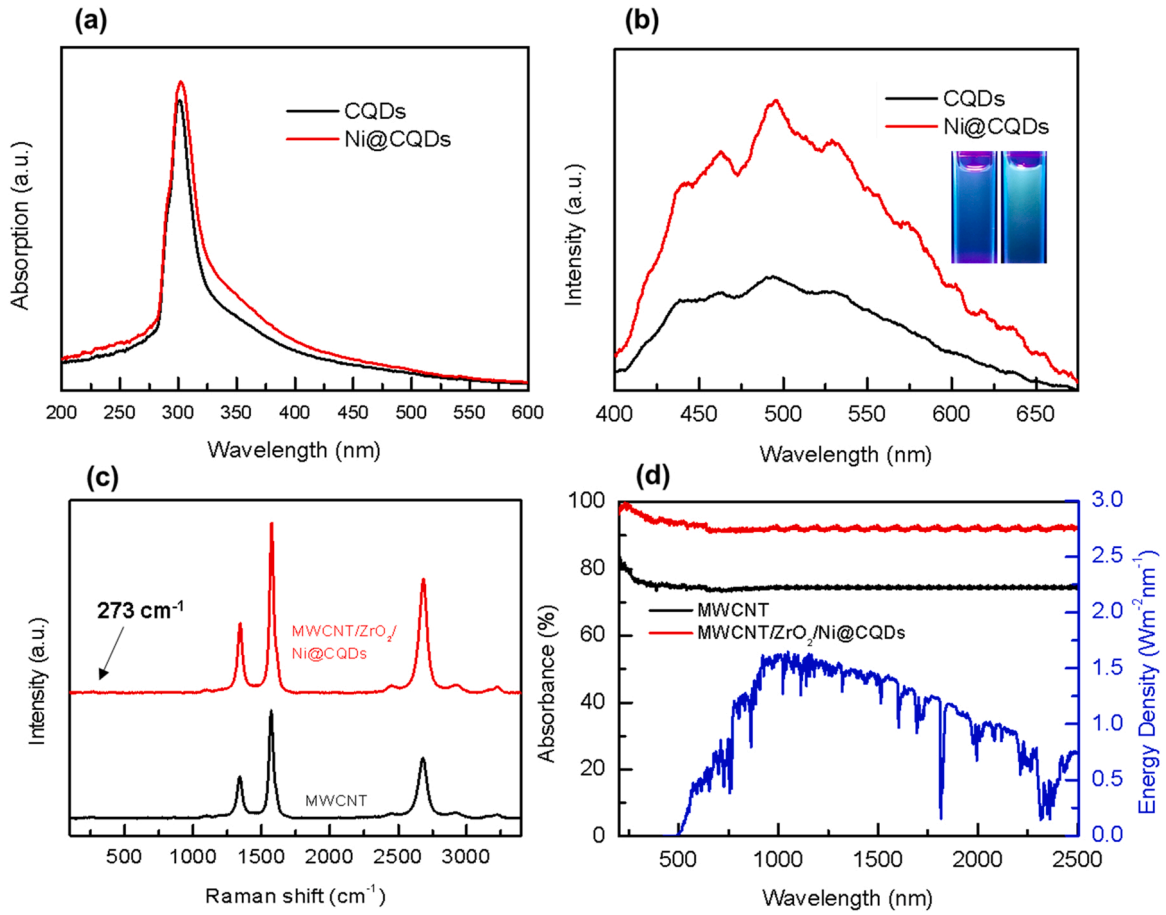

Fig. 1. (a) UV-Vis absorption, (b) fluorescence spectra of CQDs without and with Ni^{2+} ion; (c) Raman spectra and (d) Optical absorbance of MWCNT based solar absorber.

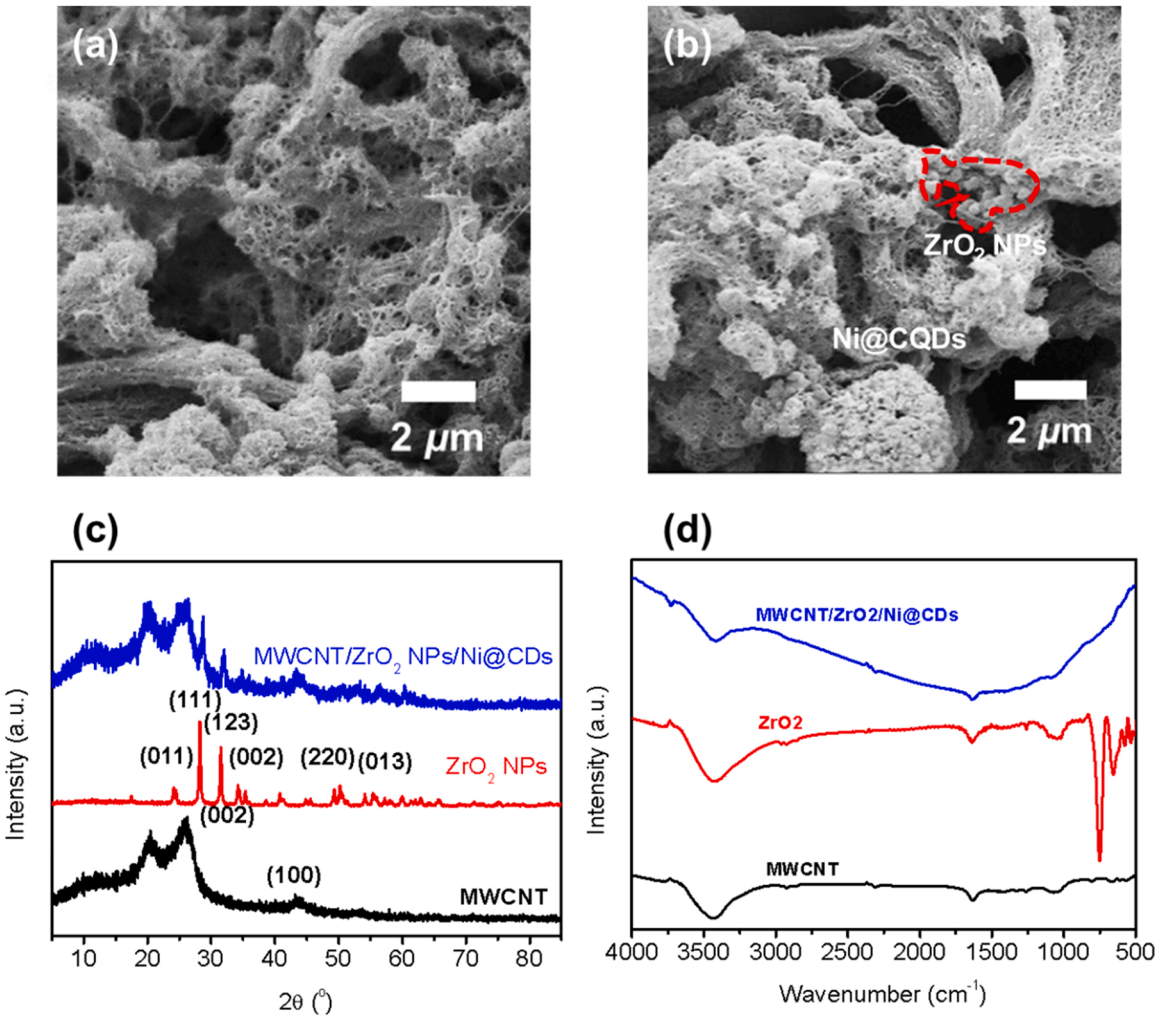

Fig. 2. SEM images of (a) MWCNT and (b) MWCNT/ZrO_2 NPs/Ni@CQDs; (c) XRD and (d) FTIR spectra of composite absorber.

2.2. Preparation of CNT/ZrO_2/Ni@CDs solar evaporators

Crab shells was cleaned with distilled water to remove impurities and dried in oven for 8 h at 90 °C. Subsequently, the dry shell crab was grinded using laboratory high speed blender until fine powder was obtained. 1 g of shell crab was mixed into 1% glacial acetic acid (70 mL), followed by ultrasonication using ultrasonic probe (Sonics VibraCell VCX750) with power of 260 W (amplitude 35%) for 1 h. For Ni@CQDs, 5 mM of $NiCl_2$ was added into above solution, followed by stirring for 30 min and hydrothermal at 150 °C for 4 h. Afterwards, the solution was centrifuged and the supernatant was collected for purification process. 50 mg of CNT and 50 mg of ZrO_2 was mixed with supernatant solution (50 mL) via ultrasonic for 1 h and the solution was heated at 180 °C for 8 h. Then, the solution was centrifuged and filtrated, followed by washing with deionized water and ethanol. Afterwards, the nanocomposite was dried in vacuum oven at 60 °C for overnight. The MWCNT (50 mg) or nanocomposite powders (50 mg) was mixed into 10 wt% PVA and the solution was heated at 90 °C for 1 h and brush coated on the surface of MF with constant weight of 30 mg, followed by drying in vacuum oven at 70 °C for 12 h.

2.3. Characterization

The optical properties of CQDs without and with Ni dopant was measured by Jenway 7315 and Ocean Optics USB 2000 + spectrometer equipped with fiber coupled LED 375 nm. Morphologies and microstructures of samples were observed with a ZEISS EVO® MA 10 scanning electron microscope (SEM) and the elemental analysis was determine using energy dispersive X-ray (EDX). The microstructural and functional groups of absorber was analyzed using x-ray diffraction (XRD) Rigaku MiniFlex and fourier transform infrared spectroscopy (FTIR) Bruker Alpha II. The surface wettability of absorber was measured using contact angle goniometer ITNANO instruments (Medan, Indonesia) with high speed mini camera. Thermal conductivity of the absorber was determine using thermal conductivity analyzer C-therm/TCi based on modified transient plane source measurement. The surface temperature of the absorber was recorded using thermal camera FLIR C2.

2.4. Solar steam generation experiments

The water evaporation were determine using custom setup based on simulated light source of halogen lamp (OSRAM 64627 HLX, Germany) at relative humidity of 48% and temperature of 28 °C. The light intensity was adjusted by the distance between the lamp and the surface of the absorber and the simulated light intensity was measured using a hand-held optical power meter. The digital analytical balance Mettler Toledo AL204 (precision 0.1 mg) was connected to PC and used for recording the mass changes of water evaporation as function of time. The thermocouple type K was used to probe the surface temperature connected to PC. The evaporation efficiency was calculated according to following equation:

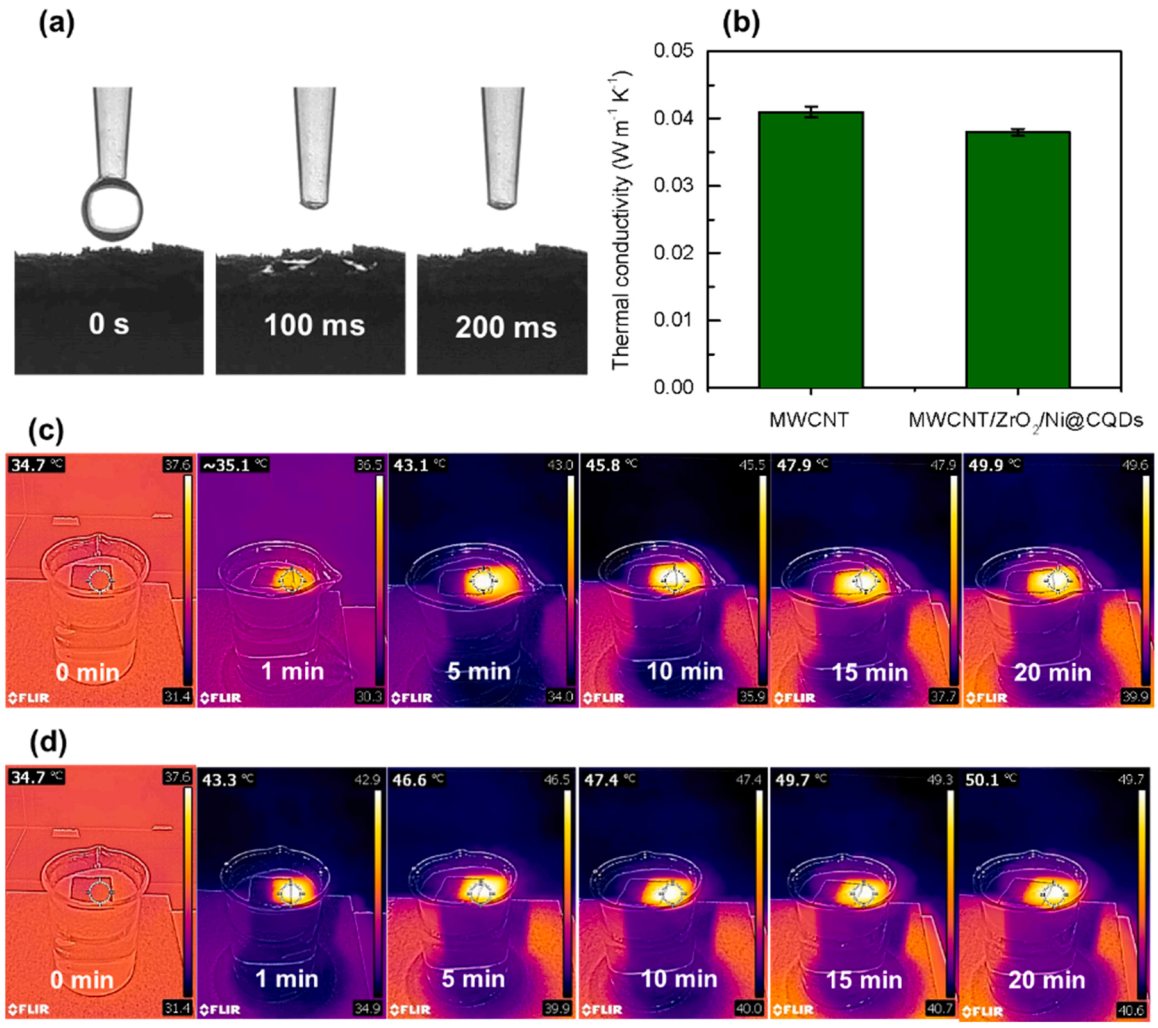

Fig. 3. (a) Time lapse photographs of water droplets onto the surface of composite absorber; (b) Thermal conductivity of the MWCNT and its composite absorber; Thermal images of surface temperature of absorber floating on beaker filled deionized water under 1-Sun exposure of (c) MWCNT and (d) MWCNT/ZrO_2 NPs/Ni@CQDs absorber, respectively.

$$\eta = \frac{m(h_{LV} + Q)}{q_i} \quad (1)$$

$$h_{LV(T)} = 1{\cdot}91846 \times 10^6 \, [T_1/(T_1\text{-}33{\cdot}91)]^2 \quad (2)$$

$$Q = C\,(T_1\text{-}T_0) \quad (3)$$

Where m refers to difference between mass changes under illumination and dark condition, h_{LV}.

(kJ kg^{-1}) represents the latent heat required to evaporate water, T_1 and T_0 is steady evaporation and initial temperature of water (K), Q means sensible heat of water of unit mass (kJ kg^{-1}) and C refers to specific heat capacity of water (4200 J kg^{-1} K^{-1}) and q_i represents energy input of light source.

3. Result and discussion

To understand the optical properties of the CQDs without and with Ni dopant, UV–vis absorption and fluorescence spectra were analyzed, respectively as shown in Fig. 1a and b. The narrow absorption peak at 300 nm and a weak shoulder at around 360 nm were correspond to the π-π * transition of aromatic sp^2 domains and n-π * transition of C═O bond, respectively [18] due to electron transitions from the carbon core. The absorption peak was shifted to 304 nm for Ni@CQDs mainly due to the Ni^{2+} arranged with surface amino groups on the CQDs. This finding is in good agreement with biomass-based CQDs [19]. As depicted in the inset of Fig. 1b, the aqueous dispersion of the CQDs were blue-green emission under UV lamp 375 nm, whereas Ni@CQDs it shows intense fluorescence at similar concentration. The strong peaks could be originated by quantum effects of CQDs modified with metal ion Ni^{2+}. The fluorescence spectra from crab shell powder showed the maximum emission wavelength at 495 nm, meanwhile the peak at 460 and 530 nm (green emission) were due to surface defects [13] and further confirmed the formation of NiO NPs on CQDs [20]. Fig. 1c present the D and G band peak located at 1341 and 1570 cm^{-1} attributed to the defects and in-plane vibration of graphite lattice, which is the main characteristics of MWCNT [21]. Interestingly, it is found that the integrated intensity ratios of D and G bands (I_D/I_G) of MWCNT increased after introduction of ZrO_2 NPs/Ni@CQDs from 0.39 to 0.51, revealing more disordered and higher defect levels. Additionally, the peak at 2676 cm^{-1} was slightly shifted to 2683 cm^{-1}, suggesting Ni@CQDs was effectively attached on MWCNT surface, meanwhile peak at 273 cm^{-1} was ascribed to the tetragonal phase of ZrO_2 [22]. Fig. 1d displayed the absorption spectra of absorber, where the average absorbance in the entire wavelength range are about 77% and 94% for MWCNT and MWCNT/ZrO_2 NPs/Ni@CQDs absorber, respectively. The MWCNT/ZrO_2 NPs/Ni@CQDs composite absorber displays the optimum optical absorption performance, which covered the solar spectrum.

SEM images of the upper surface of MF absorber with was compared

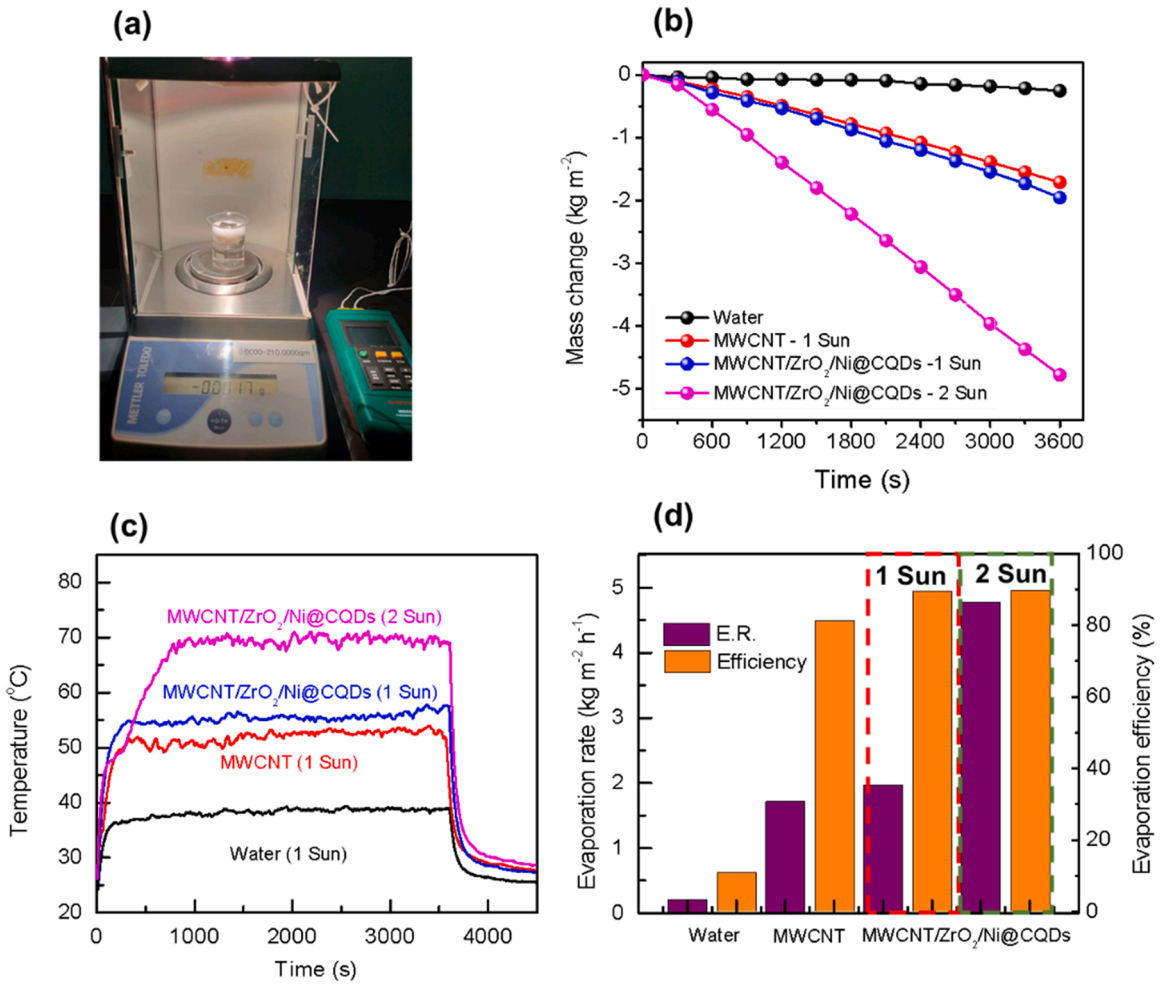

Fig. 4. (a) Physical photograph image of the solar evaporation systems for indoor system during steam generation, (b) mass changes as a function of time under 1 and 2-Sun irradiation, (c) evaporation rate and efficiency of various absorber and (d) temperature changes of absorber as a function of time.

to show the influence of ZrO_2 NPs/Ni@CQDs on the microstructure. Fig. 2a and b shows that the composite is comprised of 3D network structure with interconnected MWCNT, aggregated structure and forming a porous framework due to PVA. It can be clearly seen for the composite sample that the ZrO_2 NPs was formed between interconnection of MWCNT and the Ni@CQDs was attached on the surface of MWCNT clusters as further confirmed by elemental analysis EDX with high concentration of Ni was detected (not shown here). The crystal structure of the composite structure was determine using XRD analysis as shown in Fig. 2c. The sharp peaks in the XRD patterns of bare MWCNT at 26.28 and 43.18° attributed to the (002) and (100) planes, respectively, meanwhile peak at 20.46 ° correlated to the semicrystalline of PVA. The strong peak at 24.14, 28.22, 31.52, 34.20, 50.21 and 55.38° correspond to the (011), (111), (123), (002), (220) and (013) plane, respectively of ZrO_2 characteristics in the monoclinic phase with Ref. Code 00-024-1165 according to software analysis X′pert HighScore. Interestingly, we found that the (002) peak of MWCNT composite was slightly shifted to lower diffraction angle of 25.94°, which indicates the large lattice spacing of the CQDs edges originated by mutual repulsion between the electronegative functional groups of the CQDs [23]. This result is consistent with recent report on CQDs grown on CNT surface [24]. In addition, broad peak for composite located at 19.95° due to the presence of CQDs, meanwhile (111) plane of ZrO_2 NPs was shifted to higher angle about 0.35°, which suggests the incorporation of Ni@CQDs into the ZrO_2 and carbon framework [25]. To further understand the functional group of the composite, FTIR analysis was analyzed as shown in Fig. 2d. The intensity band at 3436 cm^{-1} associated with O–H bonds stretching of MWCNT and ZrO_2 NPs. Moreover, for ZrO_2 NPs the sharp intensity band at around 752 and 657 cm^{-1} caused by the vibrations of the Zr–O–Zr metal oxygen [26], whereas band at 1653 cm^{-1} corresponding to the carboxylate ions of ZrO_2. However, for composites sample displayed shifted to lower wavenumber due to the present of ZrO_2 NPs and Ni@CQDs. The peak at 1640 cm^{-1} attributed to the absorption of C═N/C═O [27] and the weak peak at 1078 cm^{-1} can be ascribed to the stretching vibrations of the metal-ligand bond [28].

The surface wettability of the material affects the rate of solar water evaporation. Fig. 3a exhibits the contact angle of composite absorber surface adsorbed water as function of time. The water droplet rapidly permeates completely within 200 ms into the surface of MWCNT/ZrO_2 NPs/Ni@CQDs implying the efficient water supply through the absorber layer and essential for solar-to-steam generation performance. It is noteworthy to note that there is negligible difference in surface wetting between MWCNT/ZrO_2 NPs/Ni@CQDs. This finding indicates the superhydrophilic characteristics of composite absorber, which beneficial from MF substrate [29]. Accordingly, Fig. 3b shows thermal conductivity of MWCNT and its composite are 0.04 and 0.038 W m^{-1} K^{-1}, respectively, which is extremely lower compared to normal water (~0.6 W m^{-1} K^{-1}). This result indicates the excellent thermal insulation property owing to the low thermal conductivity of ZrO_2 [30] and Ni@CQDs, the lower thermal conductivity of absorber essential for heat localization during the solar evaporation, thus promoting rapid evaporation rate. The infrared images and the surface temperature change of absorber were recorded under 1-Sun illumination by infrared thermal camera. Fig. 3c and d displayed the surface temperature increases of

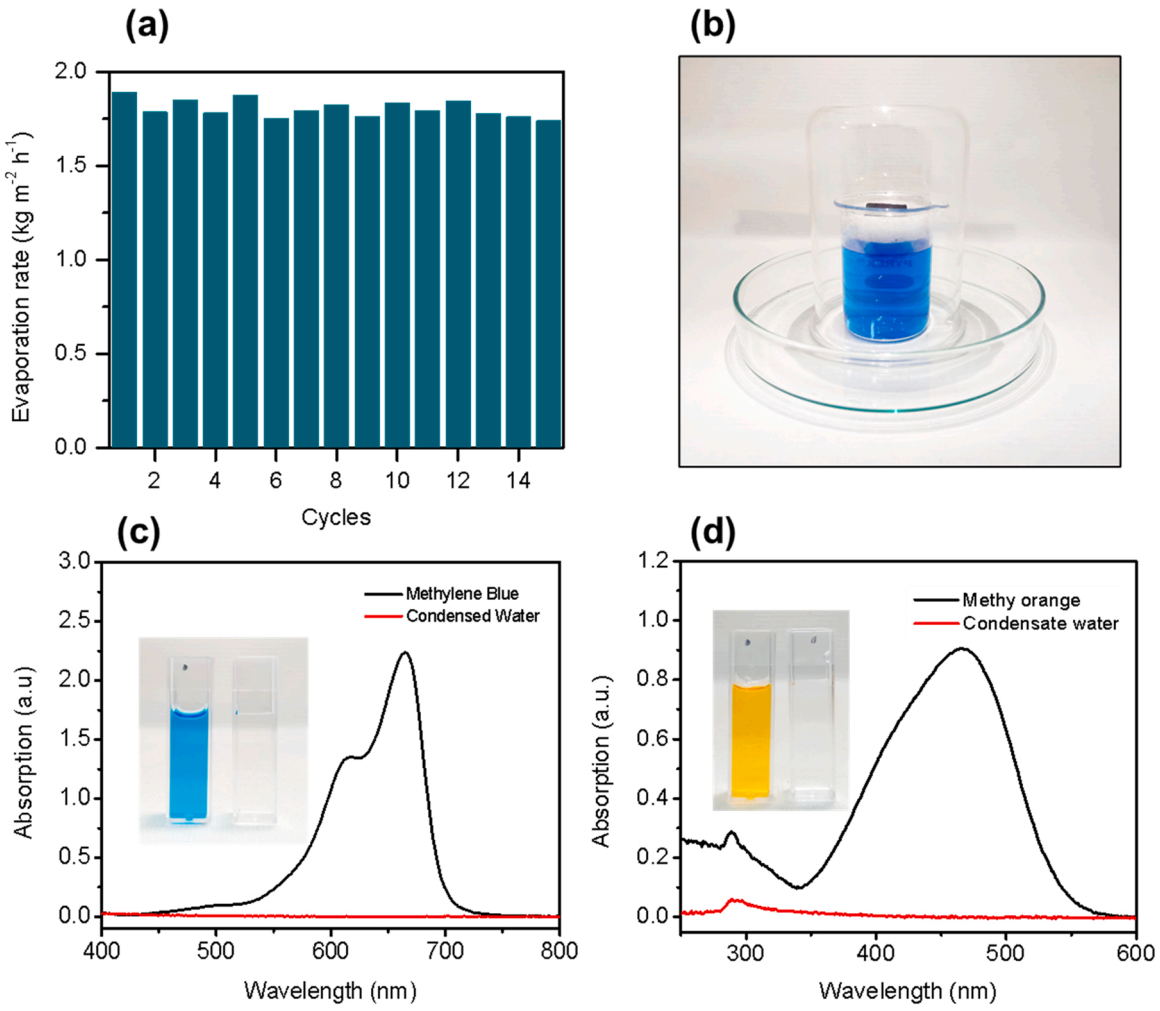

Fig. 5. (a) Evaporation rate cycle performance of solar-driven steam evaporation rates with the MWCNT/ZrO_2 NPs/Ni@CQDs composite absorber, (b) Digital photograph of experimental setup for wastewater purification; Photodegradability of (c) methylene blue and (d) methyl orange and condensed water result based on absorber under 1 Sun irradiation.

composite absorber, for the case of MWCNT/ZrO_2 NPs/Ni@CQDs, the surface temperature rose sharply from 34.7 C to 50.1 °C under 1-Sun illumination, which is slightly higher compared to MWCNT absorber. The temperature rose rapidly to 43.30 ℃ for the first 1 min, demonstrating that the MWCNT/ZrO_2 NPs/Ni@CQDs absorber potential for rapid photothermal energy conversion. Besides, this finding explained the heat localization property of the MWCNT/ZrO_2 NPs/Ni@CQDs solar steam generator and consistent with extremely low thermal conductivity.

In order to characterize the water evaporation performance, the mass changes and temperature were monitored in real time during the solar evaporation process using an analytical balance and digital thermocouple connected to a laptop were shown in Fig. 4a. Under 1 Sun irradiation, the water evaporation rates of pure water of 0.19 kg m^{-2} h^{-1}, meanwhile the solar-driven steam evaporation rates of MWCNT and MWCNT/ZrO_2 NPs/Ni@CQDs are 1.71 and 1.95 kg m^{-2} h^{-1}, which are 9 and 10 folds increment than that pure water. The evaporation rate of MWCNT/ZrO_2 NPs/Ni@CQDs absorber, which is higher than the recent report on graphene oxide (GO)/CNT of 1.30 kg m^{-2} h^{-1} [31], modified reduced GO/sodium alginate of 1.86 kg m^{-2} h^{-1} [32], carbonized towel-gourd sponges of 1.53 kg m^{-2} h^{-1} [33], MnO_2 nanowires modified CQDs of 1.68 kg m^{-2} h^{-1} [13]. There are two main reasons of the improvement of evaporation rate performance, firstly photothermal materials effectively localized heat on the surface and generate rapid increase of stabilized surface temperature to 52.82 and 57.50 °C for MWNCNT and MWCNT/ZrO_2 NPs/Ni@CQDs, respectively (Fig. 4c). In contrast, direct heating bulk water with only increase of temperature to 36.10 °C after 1 h irradiation. Secondly, MWCNT/ZrO_2 NPs/Ni@CQDs possessed lower thermal conductivity, which led to a large temperature difference between the bulk water and the absorber surface in comparison with MWCNT-only absorber. Additionally, when the light off, the surface temperature of absorber rapidly dropped, which is attributed to interfacial heating caused by the polymer insulation layer of absorber. Moreover, under 2-Sun irradiation, the evaporation rates for MWCNT/ZrO_2 NPs/Ni@CQDs absorber could reach about 4.77 kg m^{-2} h^{-1} with rapid temperature increased. In general, higher solar radiation intensity provides a larger energy density, thus leading to a increase in ratio of steam evaporation rates [34]. The solar-water evaporation efficiency o was measured by Eqs. (1–3). From Fig. 4d, the net evaporation rate of pure water, MWCNT, MWCNT/ZrO_2 NPs/Ni@CQDs absorber were summarized and the evaporation efficiency of 10.9%, 81.3% and 89.6%, respectively under 1-Sun irradiation. Further increase the solar intensity leading to evaporation efficiency of 89.8% MWCNT/ZrO_2 NPs/Ni@CQDs absorber.

The reusability and stability of the MWCNT/ZrO_2 NPs/Ni@CQDs composite absorber was subsequently confirmed by measuring the evaporation rate under 1-Sun illumination for 15 cycles. As demonstrated in Fig. 5a, the evaporation rate was maintained around 1.88 kg m^{-2} h^{-1} with a small deviation of 7%, where each cycles represents the evaporation rate of water under 1-Sun exposure for 1 h. This

result displayed the durability of the MWCNT/ZrO_2 NPs/Ni@CQDs composite absorber and implying the thermal stability and mechanically robust, which is promising for the production of clean water by solar-driven steam generation.

To understand the capability of MWCNT/ZrO_2 NPs/Ni@CQDs absorber on removing organic dyes namely, methylene blue and methyl orange as pollutants were dissolved in water with concentration of 10 mg/L. Fig. 5b displayed the experimental setup of absorber float on top of 50 mL methylene blue solution. As shown in Fig. 5c and d, the strong absorption peaks of methyl orange (464 cm) and methylene blue (664 nm) are reduced significantly (99.8%) after the solar-thermal purification as shown in the inset. This finding suggests that relatively negligible organic dyes in the purified water and demonstrate strong potential of MWCNT/ZrO_2 NPs/Ni@CQDs absorber for wastewater treatment.

4. Conclusion

In summary, excellent solar driven water evaporation performance was successfully developed via low-cost hydrothermal process of MWCNT/ZrO_2 NPs/Ni@CQDs and coated onto the surface of MF as solar absorber. The characteristics of MWCNT, ZrO2 and Ni@CQDs were determined using UV-Vis, PL, SEM, XRD and FTIR. The photothermal materials can effectively absorb 94% of wide light spectrum and demonstrate superhydrophilicity surface. The fabricated MWCNT/ZrO_2 NPs/Ni@CQDs demonstrate the highest water evaporation efficiency of 89.6% compared with MWCNT-only of 81.3%. The enhancement of efficiency can be explained due to extremely low thermal conductivity due to the addition of ZrO_2 NPs and Ni@CQDs, strong light absorption and efficient localize heat on the surface of absorber and generate rapid increase of temperature of composite absorber. In the practical wastewater purification process, organic dyes was significantly reduced with MWCNT/ZrO_2 NPs/Ni@CQDs absorber under 1 Sun irradiation. This work demonstrates an enhance yet simple strategy for development of high-performance solar-driven steam generation absorber for drinking water and wastewater purification.

CRediT authorship contribution statement

Riski Titian Ginting: Conceptualization, Methodology, Formal analysis, Writing – original draft, Writing – review & editing, Funding acquisition. **Hairus Abdullah**: Methodology, Validation, Visualization, Writing – review & editing. **Erman Taer**: Validation, Supervision. **Oktovin Purba**: Conceptualization, Writing – original draft. **Despaleri Perangin-angin**: Resources.

Declaration of Competing Interest

The authors declare that they have no known competing financial interests or personal relationships that could have appeared to influence the work reported in this paper.

Acknowledgement

The author greatly acknowledges financial support from the KEMDIKBUD, Indonesia No. 161/E4.1/AK.04. PT/2021 and 301/LL1/PG/2021.

References

[1] T.A. Larsen, S. Hoffmann, C. Lüthi, B. Truffer, M. Maurer, Emerging solutions to the water challenges of an urbanizing world, Science 352 (2016) 928–933.
[2] M. Gao, L. Zhu, C.K. Peh, G.W. Ho, Solar absorber material and system designs for photothermal water vaporization towards clean water and energy production, Energy Environ. Sci. 12 (2019) 841–864.
[3] Y. Wang, C. Wang, X. Song, M. Huang, S.K. Megarajan, S.F. Shaukat, H. Jiang, Improved light-harvesting and thermal management for efficient solar-driven water evaporation using 3D photothermal cones, J. Mater. Chem. A 6 (2018) 9874–9881.
[4] J. He, Z. Zhang, C. Xiao, F. Liu, H. Sun, Z. Zhu, W. Liang, A. Li, High-performance salt-rejecting and cost-effective superhydrophilic porous monolithic polymer foam for solar steam generation, ACS Appl. Mater. Interfaces 12 (2020) 16308–16318.
[5] Z. Huang, S. Li, X. Cui, Y. Wan, Y. Xiao, S. Tian, H. Wang, X. Li, Q. Zhao, C.-S. Lee, A broadband aggregation-independent plasmonic absorber for highly efficient solar steam generation, J. Mater. Chem. A 8 (2020) 10742–10746.
[6] I. Ibrahim, V. Bhoopal, D.H. Seo, M. Afsari, H.K. Shon, L.D. Tijing, Biomass-based photothermal materials for interfacial solar steam generation: a review, Mater. Today Energy 286 (2021), 100716.
[7] T. Yang, H. Lin, K.-T. Lin, B. Jia, Carbon-based absorbers for solar evaporation: steam generation and beyond, Sustain. Mater. Technol. 25 (2020), e00182.
[8] I. Ibrahim, D.H. Seo, A.M. McDonagh, H.K. Shon, L. Tijing, Semiconductor photothermal materials enabling efficient solar steam generation toward desalination and wastewater treatment, Desalination (2020), 114853.
[9] Q. Li, X. Zhao, L. Li, T. Hu, Y. Yang, J. Zhang, Facile preparation of polydimethylsiloxane/carbon nanotubes modified melamine solar evaporators for efficient steam generation and desalination, J. Colloid Interface Sci. 584 (2021) 602–609.
[10] G. Hu, Y. Cao, M. Huang, Q. Wu, K. Zhang, X. Lai, J. Tu, C. Tian, J. Liu, W. Huang, Salt-resistant carbon nanotubes/polyvinyl alcohol hybrid gels with tunable water transport for high-efficiency and long-term solar steam generation, Energy Technol. 8 (2020), 1900721.
[11] M.J. Molaei, The optical properties and solar energy conversion applications of carbon quantum dots: a review, Sol. Energy 196 (2020) 549–566.
[12] Q. Hou, C. Xue, N. Li, H. Wang, Q. Chang, H. Liu, J. Yang, S. Hu, Self-assembly carbon dots for powerful solar water evaporation, Carbon 149 (2019) 556–563.
[13] M.S. Irshad, X. Wang, A. Abbas, F. Yu, J. Li, J. Wang, T. Mei, J. Qian, S. Wu, M. Q. Javed, Salt-resistant carbon dots modified solar steam system enhanced by chemical advection, Carbon 176 (2021) 313–326.
[14] X. Li, J. Deng, L. Zhang, Y. Liu, H. Yue, R. Duan, D. Ge, Effect of surface textures and electrohydrodynamically atomized WS2 films on the friction and wear properties of ZrO2 coatings, Ceram. Int. 45 (2019) 1020–1030.
[15] Y. Zhao, Y. Zhang, J. Li, X. Du, Solvothermal synthesis of visible-light-active N-modified ZrO2 nanoparticles, Mater. Lett. 130 (2014) 139–142.
[16] J. He, H. Zhao, X. Li, D. Su, H. Ji, H. Yu, Z. Hu, Large-scale and ultra-low thermal conductivity of ZrO2 fibrofelt/ZrO2-SiO2 aerogels composites for thermal insulation, Ceram. Int. 44 (2018) 8742–8748.
[17] M.T. Taghizadeh, M. Vatanparast, Ultrasonic-assisted synthesis of ZrO2 nanoparticles and their application to improve the chemical stability of Nafion membrane in proton exchange membrane (PEM) fuel cells, J. Colloid Interface Sci. 483 (2016) 1–10.
[18] Y. Hu, X. Geng, L. Zhang, Z. Huang, J. Ge, Z. Li, Nitrogen-doped carbon dots mediated fluorescent on-off assay for rapid and highly sensitive pyrophosphate and alkaline phosphatase detection, Sci. Rep. 7 (2017) 1–9.
[19] Z. Liang, M. Kang, G.F. Payne, X. Wang, R. Sun, Probing energy and electron transfer mechanisms in fluorescence quenching of biomass carbon quantum dots, ACS Appl. Mater. Interfaces 8 (2016) 17478–17488.
[20] S.J. Musevi, A. Aslani, H. Motahari, H. Salimi, Offer a novel method for size appraise of NiO nanoparticles by PL analysis: synthesis by sonochemical method, J. Saudi Chem. Soc. 20 (2016) 245–252.
[21] Y. Piao, V.N. Tondare, C.S. Davis, J.M. Gorham, E.J. Petersen, J.W. Gilman, K. Scott, A.E. Vladár, A.R.H. Walker, Comparative study of multiwall carbon nanotube nanocomposites by Raman, SEM, and XPS measurement techniques, Compos. Sci. Technol. 208 (2021), 108753.
[22] S. Ratnayake, M. Mantilaka, C. Sandaruwan, D. Dahanayake, E. Murugan, S. Kumar, G. Amaratunga, K.N. de Silva, Carbon quantum dots-decorated nano-zirconia: a highly efficient photocatalyst, Appl. Catal. A Gen. 570 (2019) 23–30.
[23] J. Peng, W. Gao, B.K. Gupta, Z. Liu, R. Romero-Aburto, L. Ge, L. Song, L. B. Alemany, X. Zhan, G. Gao, Graphene quantum dots derived from carbon fibers, Nano Lett. 12 (2012) 844–849.
[24] M. Ali, A.S. Anjum, R. Riaz, A. Bibi, K.C. Sun, S.H. Jeong, Unraveling the surface states related Stokes shift dependent electrocatalytic activity of N-doped carbon quantum dots for photovoltaic applications, Carbon 181 (2021) 155–168.
[25] B. Tian, S. Liu, L. Feng, S. Liu, S. Gai, Y. Dai, L. Xie, B. Liu, P. Yang, Y. Zhao, Renal-clearable nickel-doped carbon dots with boosted photothermal conversion efficiency for multimodal imaging-guided cancer therapy in the second near-infrared biowindow, Adv. Funct. Mater. 31 (2021), 2100549.
[26] F. Ordóñez, F. Chejne, E. Pabón, K. Cacua, Synthesis of ZrO2 nanoparticles and effect of surfactant on dispersion and stability, Ceram. Int. 46 (2020) 11970–11977.
[27] X. Miao, D. Qu, D. Yang, B. Nie, Y. Zhao, H. Fan, Z. Sun, Synthesis of carbon dots with multiple color emission by controlled graphitization and surface functionalization, Adv. Mater. 30 (2018), 1704740.
[28] Y. Ma, Y. Cen, M. Sohail, G. Xu, F. Wei, M. Shi, X. Xu, Y. Song, Y. Ma, Q. Hu, A ratiometric fluorescence universal platform based on N, Cu codoped carbon dots to detect metabolites participating in H2O2-generation reactions, ACS Appl. Mater. Interfaces 9 (2017) 33011–33019.
[29] Z. Xu, K. Miyazaki, T. Hori, Dopamine-induced superhydrophobic melamine foam for oil/water separation, Adv. Mater. Interfaces 2 (2015), 1500255.
[30] H. Yu, Z. Tong, Y. Qiao, Z. Yang, S. Yue, X. Li, D. Su, H. Ji, High thermal stability of sio2–zro2 aerogels using solvent-thermal aging, J. Solid State Chem. 291 (2020), 121624.

[31] L. Li, L. Zang, S. Zhang, T. Dou, X. Han, D. Zhao, Y. Zhang, L. Sun, Y. Zhang, GO/CNT-silica Janus nanofibrous membrane for solar-driven interfacial steam generation and desalination, J. Taiwan Inst. Chem. Eng. 111 (2020) 191–197.
[32] H. Jian, Y. Wang, W. Li, Y. Ma, W. Wang, D. Yu, Reduced graphene oxide aerogel with the dual-cross-linked framework for efficient solar steam evaporation, Colloids Surf. A Physicochem. Eng. Asp. 629 (2021), 127440.
[33] X. Shan, A. Zhao, Y. Lin, Y. Hu, Y. Di, C. Liu, Z. Gan, Low-cost, scalable, and reusable photothermal layers for highly efficient solar steam generation and versatile energy conversion, Adv. Sustain. Syst. 4 (2020), 1900153.
[34] X. Zhou, F. Zhao, Y. Guo, Y. Zhang, G. Yu, A hydrogel-based antifouling solar evaporator for highly efficient water desalination, Energy Environ. Sci. 11 (2018) 1985–1992.